Journal of Vibration and Control

Vibrations of Mindlin Sectorial Plates Using the Ritz Method Considering Stress Singularities

C. S. Huang, M. J. Chang and A. W. Leissa

The online version of this article can be found at:

Published by:

$SAGE

http://www.sagepublications.com

Additional services and information for *Journal of Vibration and Control* can be found at:

Email Alerts: http://jvc.sagepub.com/cgi/alerts

Subscriptions: http://jvc.sagepub.com/subscriptions

Reprints: http://www.sagepub.com/journalsReprints.nav

Permissions: http://www.sagepub.com/journalsPermissions.nav

Citations: http://jvc.sagepub.com/content/12/6/635.refs.html

>> Version of Record - May 24, 2006

What is This?

Vibrations of Mindlin Sectorial Plates Using the Ritz Method Considering Stress Singularities

C. S. HUANG

M. J. CHANG
Department of Civil Engineering, National Chiao Tung University, 1001 Ta-Hsueh Rd., Hsinchu, Taiwan 30050 (cshuang@mail.nctu.edu.tw)

A. W. LEISSA
Colorado State University, Fort Collins, Colorado, USA

Abstract: This paper reports very accurate vibration frequencies of moderately thick sectorial plates with various boundary conditions and vertex angles ($\alpha = 90°$, $180°$, $270°$, $300°$, $330°$, and $355°$) based on Mindlin plate theory, and provides the nodal patterns of their vibration modes for the first time in the published literature. Most of the extensive frequencies presented are exact to the four digits shown. The classical Ritz method is employed, using corner functions and algebraic trigonometric functions as the admissible functions. Because the corner functions properly describe the singularity behaviors of moments and shear forces in the vicinity of the vertex of a sectorial plate, they substantially enhance the convergence and accuracy of the numerical results, which is shown by convergence studies.

1. INTRODUCTION

Plates are fundamental structural components, which are widely used in practical engineering projects and have caught many researchers' interests. Leissa (1969, 1977a, 1977b, 1981a, 1981b, 1987a, 1987b) reviewed more than one thousand technical publications on vibrations of thin or thick plates published before 1985, while Liew et al. (1995) concentrated their review on the vibrations of thick plates on pre-1994 publications. These reviews show that there are far fewer studies on vibrations of sectorial plates than for circular, rectangular, or even annular sector plates. The existence of moment and shear force singularities at the vertex of a sectorial plate considerably increases the difficulty of numerically obtaining accurate frequencies and mode shapes for this configuration.

A number of studies have been carried out on vibrations of thin sectorial plates. Based on classical thin plate theory, Huang et al. (1993) provided the first known exact analytical solution for sectorial plates with simply supported radial edges. No exact analytical solutions are possible with other boundary conditions along the radial edges. Various numerical solutions were developed, such as those based on energy methods (Rubin, 1975; Bhattacharya and Bhowmic, 1975), finite element method (Houmat, 2001), finite strip method (Cheung and Chan, 1981), differential quadrature method (Wang and Wang, 2004), and the Ritz method

(Leissa et al., 1993; McGee et al., 2003). Among these numerical solutions for thin plates, the solutions developed by Leissa et al. (1993) and McGee et al. (2003) are the most accurate because the admissible functions in the Ritz method include the corner functions, which appropriately describe the singular behavior of moments in the neighborhood of the vertex of a sectorial plate. Experimental studies were also performed by Waller (1952) and Maruyama and Ichinomiya (1981) into the vibration behavior of free and clamped sectorial plates, respectively.

Only a few investigations have been carried out into the vibrations of sectorial plates based on Mindlin or Reissner plate theory, even though shear deformation and rotary inertia are known to be important to any analysis of moderately thick plates, and in determining the higher vibration frequencies of thin plates. Huang et al. (1994) obtained exact analytical solutions for sectorial plates with simply supported radial edges, which involve ordinary and modified Bessel functions. Liu and Liew (1999) applied the differential quadrature method to analyze the free vibration of sectorial plates with edges either clamped or simply supported. They considered annular sector plates with an inner to outer radius ratio of 0.00001 and with free boundary conditions along the inner circular edge, so that no moment and shear force singularities need to be taken into account. This was the same procedure used earlier by Leissa et al. (1993) for thin annular plates, presented there in addition to the method employing corner functions. The accuracy of this approach depends on the inner to outer radius ratio chosen and the boundary conditions along the inner circular edge. While a number of researchers have investigated vibrations of thick annular sector plates using various methods (e.g., Guruswamy and Yang, 1979; Cheung and Chan, 1981; Srinivasan and Thiruvenkatachari, 1985; Mizusawa, 1991; Xiang et al., 1993; Mizusawa et al., 1994; McGee et al., 1995a; Liew and Liu, 2000), only Xiang et al. (1993) demonstrated results for plates with an inner to outer radius ratio of 0.00001 and with sector angles not larger than 90°.

The studies cited above reveal that there is a need to develop accurate solutions for vibration frequencies of thick sectorial plates with various boundary conditions and vertex angles, and which may have moment and shear force singularities at the neighborhood of the vertex of the sectorial plate. In the present work, a procedure recently developed for the analysis of skewed plates with re-entrant corners (Huang et al., 2005) is extended to sectorial plates. The Ritz method is used with displacement components, which are represented by a mathematically complete set of admissible algebraic-trigonometric polynomials in conjunction with corner functions that appropriately represent the singular behaviors of moments and shear forces in the neighborhood of the vertex. The corner functions significantly accelerate the convergence of the numerical solutions. Accurate non-dimensional frequencies are presented for sectorial plates with various boundary conditions, vertex angles ($\alpha = 90°$, $180°$, $270°$, $300°$, $330°$, and $355°$), and thickness-to-radius ratios ($h/a = 0.1$ or 0.2). The nodal patterns are also shown.

2. METHODOLOGY

In the Ritz method, the vibration frequencies of plates are obtained by minimizing the energy function
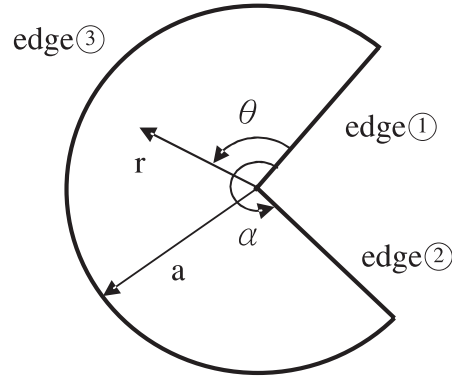
$$\Pi = V_{\max} - T_{\max}, \tag{1}$$

Figure 1. Geometry and coordinate system of a sectorial plate.

where $V_{\max}$ and $T_{\max}$ are maximum strain energy and maximum kinetic energy during a vibratory cycle, respectively. In terms of polar coordinates (see Figure 1), $V_{\max}$ and $T_{\max}$ are expressed as

$$T_{\max} = \frac{\omega^2 \rho}{2} \left[\frac{h^3}{12} \iint (\psi_r^2 + \psi_\theta^2) dA + h \iint w^2 dA \right], \tag{2}$$

$$
\begin{aligned}
V_{\max} = \frac{1}{2} \iint_A \Bigg\{ & D \left[\left(\psi_{r,r} + \frac{1}{r}\psi_r + \frac{1}{r}\psi_{\theta,\theta} \right)^2 - 2(1-\upsilon)\frac{1}{r}\psi_{r,r}(\psi_{\theta,\theta} + \psi_r) \right. \\
& + \left. \frac{1}{2}(1-\upsilon)\left(\psi_{\theta,r} + \frac{1}{r}\psi_{r,\theta} - \frac{1}{r}\psi_\theta \right)^2 \right] \\
& + \kappa^2 Gh \left[(\psi_r + w_{,r})^2 + \left(\psi_\theta + \frac{1}{r}w_{,\theta} \right)^2 \right] \Bigg\} dA,
\end{aligned}
\tag{3}
$$

where w is the transverse displacement of the mid-plane, ψ_r and ψ_θ are the bending rotations of the mid-plane normal in the r and θ directions respectively, h is the thickness of the plate, $D = Eh^3/12(1 - \upsilon^2)$ is the flexural rigidity, E is the modulus of elasticity, υ is Poisson's ratio, κ^2 is the shear correction factor, G is the shear modulus, ρ is the density of the plate, and ω is a free vibration frequency.

The admissible functions for displacement components are assumed as the sum of two sets of functions,

$$\psi_r(r,\theta) = \Psi_{r\,p}(r,\theta) + \Psi_{r\,c}(r,\theta), \tag{4a}$$

$$\psi_\theta(r,\theta) = \Psi_{\theta\,p}(r,\theta) + \Psi_{\theta\,c}(r,\theta), \tag{4b}$$

$$w(r,\theta) = W_p(r,\theta) + W_c(r,\theta), \tag{4c}$$

where Ψ_{rp}, $\Psi_{\theta p}$ and W_p consist of algebraic-trigonometric polynomials, and Ψ_{rc}, $\Psi_{\theta c}$ and W_c are three sets of corner functions accounting for the singular behaviors of moments and shear forces at the vertex. The algebraic-trigonometric polynomials are expressed as

$$
\begin{aligned}
\Psi_{rp}(r,\theta) &= g_1(r)\left\{ f_1(\theta)\left[\sum_{i=2,4}^{I_1}\sum_{j=2,4}^{i} B_{ij}r^{i-1}\cos j\theta + \sum_{i=3,5}^{I_2}\sum_{j=1,3}^{i} B_{ij}r^{i-1}\cos j\theta\right]\right.\\
&\quad + \left. f_2(\theta)\left[\sum_{i=2,4}^{I_3}\sum_{j=2,4}^{i} \tilde{B}_{ij}r^{i-1}\sin j\theta + \sum_{i=3,5}^{I_4}\sum_{j=1,3}^{i} \tilde{B}_{ij}r^{i-1}\sin j\theta\right]\right\},
\end{aligned}
\tag{5a}
$$

$$
\begin{aligned}
\Psi_{\theta p}(r,\theta) &= g_2(r)\left\{ f_3(\theta)\left[\sum_{i=2,4}^{I_1}\sum_{j=2,4}^{i} C_{ij}r^{i-1}\cos j\theta + \sum_{i=3,5}^{I_2}\sum_{j=1,3}^{i} C_{ij}r^{i-1}\cos j\theta\right]\right.\\
&\quad + \left. f_4(\theta)\left[\sum_{i=2,4}^{I_3}\sum_{j=2,4}^{i} \tilde{C}_{ij}r^{i-1}\sin j\theta + \sum_{i=3,5}^{I_4}\sum_{j=1,3}^{i} \tilde{C}_{ij}r^{i-1}\sin j\theta\right]\right\},
\end{aligned}
\tag{5b}
$$

$$
\begin{aligned}
W_p(r,\theta) &= g_3(r)\left\{ f_5(\theta)\left[\sum_{i=0,2,4}^{I_5}\sum_{j=0,2,4}^{i} A_{ij}r^{i}\cos j\theta + \sum_{i=1,3}^{I_6}\sum_{j=1,3}^{i} A_{ij}r^{i}\cos j\theta\right]\right.\\
&\quad + \left. f_6(\theta)\left[\sum_{i=2,4}^{I_7}\sum_{j=2,4}^{i} \tilde{A}_{ij}r^{i}\sin j\theta + \sum_{i=1,3}^{I_8}\sum_{j=1,3}^{i} \tilde{A}_{ij}r^{i}\sin j\theta\right]\right\},
\end{aligned}
\tag{5c}
$$

where A_{ij}, B_{ij}, C_{ij}, $\tilde{A}_{ij}$, $\tilde{B}_{ij}$ and $\tilde{C}_{ij}$ are coefficients to be determined by minimizing Π. In equations (5), I_k can be different for different k. However, for simplicity, they are set to be $I_1 = I_3 = I_5 = I_7$ and $I_2 = I_4 = I_6 = I_8$ in the following. Functions $g_i(r)$ and $f_j(\theta)$ are chosen to make the admissible functions satisfy the geometric boundary conditions along the circular and radial edges, respectively.

For different boundary conditions along the circular edge ($r = a$), $g_i(r)$ are chosen as follows:

Clamped : $g_i(r) = (1 - r/a)$ for $i = 1, 2,$ and 3;

Simply supported : $g_2(r) = g_3(r) = (1 - r/a)$, and $g_1(r) = 1$;

Free : $g_i(r) = 1$ for $i = 1, 2,$ and 3.

Functions $f_j(\theta)$ ($j = 1, 2, \ldots, 6$) are expressed as

$$
f_j(\theta) = \theta^{m_j}(1 - \theta/\alpha)^{n_j},
\tag{6}
$$

where m_j and n_j are either zero or one depending on the boundary conditions along the radial edges. For different boundary conditions along $\theta = 0$, m_j is given as follows:

$$\text{Clamped}: \quad m_1 = m_3 = m_5 = 1, \text{ the rest all equal to zero};$$

$$\text{Simply supported}: \quad m_1 = m_5 = 1, \text{ the rest all equal to zero};$$

$$\text{Free}: \quad \text{all equal to zero}.$$

The same rule is applied to n_j for different boundary conditions along $\theta = \alpha$. Notably, the simply supported conditions given above simulate the mechanical support of a line hinge along an edge.

When the problems under consideration are symmetric (i.e., have the same boundary conditions along the two radial edges), one can take advantage of the symmetry and set $\theta = 0$ as the symmetry axis. Then functions $f_j(\theta)$ ($j = 1, 2, \ldots, 6$) can expressed as

$$f_j(\theta) = (1 + 2\theta/\alpha)^{k_j}(1 - 2\theta/\alpha)^{k_j}, \tag{7}$$

where the rule for determining k_j is the same as that for m_j given above.

The sets of corner functions are written as

$$\Psi_{rc}(r,\theta) = g_1(r)\sum_{k=1}^{K}\left[\overline{B}_k\,\text{Re}(\overline{\Psi}_{rk}(r,\theta,\lambda_k)) + \hat{B}_k\,\text{Im}(\overline{\Psi}_{rk}(r,\theta,\lambda_k))\right], \tag{8a}$$

$$\Psi_{\theta c}(r,\theta) = g_2(r)\sum_{k=1}^{K}\left[\bar{C}_k\,\text{Re}(\overline{\Psi}_{\theta k}(r,\theta,\lambda_k)) + \hat{C}_k\,\text{Im}(\overline{\Psi}_{\theta k}(r,\theta,\lambda_k))\right], \tag{8b}$$

$$W_c(r,\theta) = g_3(r)\sum_{l=1}^{L}\overline{A}_l\overline{W}_l(r,\theta,\lambda_k), \tag{8c}$$

where $\overline{\Psi}_{r\,k}$, $\overline{\Psi}_{\theta\,k}$ and $\overline{W}_l$ are established from the asymptotic solutions presented by Huang (2003) and McGee et al. (2005). The expressions for $\overline{\Psi}_{r\,k}$, $\overline{\Psi}_{\theta\,k}$ and $\overline{W}_l$ used in this work are listed in Table 1. When λ_k in Table 1 is a complex number, the corresponding $\overline{\Psi}_{r\,k}$ and $\overline{\Psi}_{\theta\,k}$ are complex functions. Because $\bar{\lambda}_k$ is always real, $\overline{W}_k$ is a real function. To meet the regularity conditions at $r = 0$ the real parts of λ_k and $\bar{\lambda}_k$ have to exceed zero, and λ_k and $\bar{\lambda}_k$ are ranked by increasing order of magnitude of the real part. $\overline{\Psi}_{r\,k}$ and $\overline{\Psi}_{\theta\,k}$ are usually more complicated than the algebraic-trigonometric polynomials used in $\overline{\Psi}_{r\,p}$ and $\overline{\Psi}_{\theta\,p}$.

Using the Ritz method, the free vibration problem is solved by substituting equations (4), (5) and (8) into equations (2) and (3), and minimizing the energy functional Π given in equation (1) with respect to the coefficients A_{ij}, B_{ij}, C_{ij}, $\tilde{A}_{ij}$, $\tilde{B}_{ij}$, $\tilde{C}_{ij}$, $\overline{A}_l$, $\overline{B}_k$, $\bar{C}_k$, $\hat{B}_k$, and $\hat{C}_k$ by partial differentiation. This yields a set of homogeneous linear algebraic equations in terms of these coefficients, which lead to a standard eigenvalue problem. A similar formulation for these equations in matrix form can be found in Xiang et al. (1993). The resulting eigenvalues correspond to the vibration frequencies, and the corresponding eigenfunctions describe the mode shapes.

Table 1. Corner functions corresponding to various boundary conditions along radial edges.

Boundary conditions along radial edges	Corner functions
Clamped-Free	$\overline{\Psi}_{rk}(r,\theta) = r^{\lambda_k}\{\cos(\lambda_k+1)\theta - \bar{k}_1\eta_1\sin(\lambda_k+1)\theta - \cos(\lambda_k-1)\theta$ $+\eta_1\sin(\lambda_k-1)\theta\},$ $\overline{\Psi}_{\theta k}(r,\theta) = r^{\lambda_k}\{-\sin(\lambda_k+1)\theta - \bar{k}_1\eta_1\cos(\lambda_k+1)\theta + \bar{k}_1\sin(\lambda_k-1)\theta$ $+\bar{k}_1\eta_1\cos(\lambda_k-1)\theta\},$ $\overline{W}_k(r,\theta) = r^{\bar{\lambda}_k}\sin\bar{\lambda}_k\theta,$ where $$\eta_1 = -\frac{\lambda_k(1-\upsilon)\cos(\lambda_k+1)\alpha - (\bar{k}_1(\lambda_k-1)-\lambda_k\upsilon-1)\cos(\lambda_k-1)\alpha}{(\bar{k}_1(\lambda_k-1)-\lambda_k\upsilon-1)\sin(\lambda_k-1)\alpha - \bar{k}_1\lambda_k(1-\upsilon)\sin(\lambda_k+1)\alpha}$$ $\bar{k}_1 = -\dfrac{[2(1-\upsilon)+(1+\upsilon)(\lambda_k+1)]}{[2(1-\upsilon)-(1+\upsilon)(\lambda_k-1)]}$, and λ_k and $\bar{\lambda}_k$ are the kth root of $$\sin^2\lambda\alpha = \frac{4-\lambda^2(1+\upsilon)^2\sin^2\alpha}{(3-\upsilon)(1+\upsilon)} \text{ and } \cos\bar{\lambda}\alpha = 0, \text{ respectively.}$$
Simply supported-Free	$\overline{\Psi}_{rk}(r,\theta) = r^{\lambda_k}\{\eta_2\sin(\lambda_k+1)\theta + \sin(\lambda_k-1)\theta\},$ $\overline{\Psi}_{\theta k}(r,\theta) = r^{\lambda_k}\{\eta_2\cos(\lambda_k+1)\theta + \bar{k}_1\cos(\lambda_k-1)\theta\},$ $\overline{W}_k(r,\theta) = r^{\bar{\lambda}_k}\sin\bar{\lambda}_k\theta,$ where $\eta_2 = -\dfrac{(1+\lambda)(1+\upsilon)}{-3+\lambda+\upsilon+\lambda\upsilon}\dfrac{\sin(\lambda-1)\alpha}{\sin(\lambda+1)\alpha}$, and λ_k and $\bar{\lambda}_k$ are the kth root of $\sin 2\lambda\alpha = \lambda\sin 2\alpha$ and $\cos\bar{\lambda}\alpha = 0$, respectively.
Simply supported-Clamped	$\overline{\Psi}_{rk}(r,\theta) = r^{\lambda_k}\left\{-\dfrac{\sin(\lambda_k-1)\alpha}{\sin(\lambda_k+1)\alpha}\sin(\lambda_k+1)\theta + \sin(\lambda_k-1)\theta\right\},$ $\overline{\Psi}_{\theta k}(r,\theta) = r^{\lambda_k}\left\{-\dfrac{\sin(\lambda_k-1)\alpha}{\sin(\lambda_k+1)\alpha}\cos(\lambda_k+1)\theta + \bar{k}_1\cos(\lambda_k-1)\theta\right\},$ $\overline{W}_k(r,\theta) = r^{\bar{\lambda}_k}\sin\bar{\lambda}_k\theta,$ where λ_k and $\bar{\lambda}_k$ are the kth root of $$\sin 2\lambda\alpha = \frac{\lambda(1+\upsilon)}{-3+\upsilon}\sin 2\alpha \text{ and } \sin\bar{\lambda}\alpha = 0, \text{ respectively.}$$
Free-Free	(1) Symmetric case $\overline{\Psi}_{rk}(r,\theta) = r^{\lambda_k}\{\eta_3\cos(\lambda_k+1)\theta + \cos(\lambda_k-1)\theta\}$ $\overline{\Psi}_{\theta k}(r,\theta) = r^{\lambda_k}\{-\eta_3\sin(\lambda_k+1)\theta - \bar{k}_1\sin(\lambda_k-1)\theta\}$ $\overline{W}_k(r,\theta) = r^{\bar{\lambda}_k}\cos\bar{\lambda}_k\theta$ where $\eta_3 = -\dfrac{\bar{k}_1(\lambda_k-1)-\lambda_k\upsilon-1}{\lambda_k(1-\upsilon)}\dfrac{\cos(\lambda_k-1)\alpha/2}{\cos(\lambda_k+1)\alpha/2}$, and λ_k and $\bar{\lambda}_k$ are the kth root of $\sin\lambda\alpha = -\lambda\sin\alpha$ and $\sin\bar{\lambda}\alpha/2 = 0$, respectively.

Table 1. Corner functions corresponding to various boundary conditions along radial edges. *(Continued)*

Boundary conditions along radial edges	Corner functions
	(2) Antisymmetric case $\overline{\Psi}_{rk}(r,\theta) = r^{\lambda_k}\{\eta_4 \sin(\lambda_k + 1)\theta + \sin(\lambda_k - 1)\theta\}$ $\overline{\Psi}_{\theta k}(r,\theta) = r^{\lambda_k}\{\eta_4 \cos(\lambda_k + 1)\theta + \bar{k}_1 \cos(\lambda_k - 1)\theta\}$ $W_k(r,\theta) = r^{\bar{\lambda}_k} \sin \bar{\lambda}_k \theta$ where $\eta_4 = -\dfrac{\bar{k}_1(\lambda_k - 1) - \lambda_k \upsilon - 1}{\lambda_k(1 - \upsilon)}\dfrac{\sin(\lambda_k - 1)\alpha/2}{\sin(\lambda_k + 1)\alpha/2}$, and λ_k and $\bar{\lambda}_k$ are the kth root of $\sin \lambda\alpha = \lambda \sin \alpha$ and $\cos \bar{\lambda}\alpha/2 = 0$, respectively.
Clamped- Clamped	(1) Symmetric case: $\overline{\Psi}_{rk}(r,\theta) = r^{\lambda_k}\left\{\cos(\lambda_k + 1)\theta - \left(\dfrac{\cos(\lambda_k + 1)\alpha/2}{\cos(\lambda_k - 1)\alpha/2}\right)\cos(\lambda_k - 1)\theta\right\}$ $\overline{\Psi}_{\theta k}(r,\theta) = r^{\lambda_k}\left\{-\sin(\lambda_k + 1)\theta + \bar{k}_1\left(\dfrac{\cos(\lambda_k + 1)\alpha/2}{\cos(\lambda_k - 1)\alpha/2}\right)\sin(\lambda_k - 1)\theta\right\}$ $W_k(r,\theta) = r^{\bar{\lambda}_k} \cos \bar{\lambda}_k \theta$ where λ_k and $\bar{\lambda}_k$ are the kth root of $\sin \lambda\alpha = -\dfrac{\lambda(1 + \upsilon)}{-3 + \upsilon}\sin \alpha$ and $\cos \bar{\lambda}\alpha/2 = 0$, respectively.
	(2) Antisymmetric case $\overline{\Psi}_{rk}(r,\theta) = r^{\lambda_k}\left\{\sin(\lambda_k + 1)\theta - \left(\dfrac{\sin(\lambda_k + 1)\alpha/2}{\sin(\lambda_k - 1)\alpha/2}\right)\sin(\lambda_k - 1)\theta\right\}$ $\overline{\Psi}_{\theta k}(r,\theta) = r^{\lambda_k}\left\{\cos(\lambda_k + 1)\theta - \bar{k}_1\left(\dfrac{\sin(\lambda_k + 1)\alpha/2}{\sin(\lambda_k - 1)\alpha/2}\right)\cos(\lambda_k - 1)\theta\right\}$ $\overline{W}_k(r,\theta) = r^{\bar{\lambda}_k} \sin \bar{\lambda}_k \theta$ where λ_k and $\bar{\lambda}_k$ are the kth root of $\sin \lambda\alpha = \dfrac{\lambda(1 + \upsilon)}{-3 + \upsilon}\sin \alpha$ and $\sin \bar{\lambda}_k\alpha/2 = 0$, respectively.

3. CONVERGENCE STUDIES

The Ritz method always gives upper-bound solutions for vibration frequencies. Because the sets of polynomials (equations (5)) are mathematically complete, the numerical solutions will converge to exact solutions when the number of admissible functions is sufficiently large. The purpose of the corner functions (equations (8)) is to accelerate the convergence. Here, convergence studies were conducted to verify the accuracy of the present solutions and

Table 2. Convergence of $\omega a^2 \sqrt{\rho h/D}$ for a sectorial plate with C-F-F boundary conditions and $\alpha = 90°$.

Mode no.	No. of corner functions	(I_{even},I_{odd}) in Eqs.(5)				
		(16,15)	(18,17)	(20,19)	(22,21)	(22,23)
	($\Psi_{r\,c}$, $\Psi_{\theta\,c}$, W_c)	437[#]	546[#]	667[#]	800[#]	872[#]
1	(0,0,0)	4.466	4.432	4.419	4.415	4.412
	(10,10,10)	4.427	4.416	4.409	4.403	4.402
	(20,20,20)	4.414	4.407	4.402	4.400	4.400
2	(0,0,0)	12.88	12.78	12.73	12.73	12.72
	(10,10,10)	12.76	12.74	12.72	12.71	12.71
	(20,20,20)	12.73	12.72	12.71	12.71	12.71
3	(0,0,0)	23.22	23.17	23.12	23.08	23.08
	(10,10,10)	23.15	23.11	23.07	23.07	23.06
	(20,20,20)	23.10	23.07	23.06	23.06	23.06
4	(0,0,0)	32.42	32.27	32.23	32.22	32.21
	(10,10,10)	32.27	32.23	32.21	32.20	32.20
	(20,20,20)	32.22	32.21	32.20	32.20	32.20
5	(0,0,0)	48.01	47.87	47.81	47.80	47.78
	(10,10,10)	47.89	47.85	47.80	47.77	47.77
	(20,20,20)	47.81	47.79	47.77	47.77	47.77

Note: "#" denotes the total number of terms in Ψ_{rp}, $\Psi_{\theta p}$ and W_p.

to show the effects of corner functions on the numerical solutions. The results given here are for plates with $\upsilon = 0.3$ and κ^2 (shear correction factor) $= \pi^2/12$.

The different combinations of boundary conditions along radial edges and circular edge are considered in this section and the next are F-F-F, C-F-F, S-F-F, C-C-F, S-C-F, and C-C-C (where S-C-F, for instance, denotes simply supported, clamped, and free boundary conditions along edges 1, 2, and 3, respectively, on the sectorial plate shown in Figure 1).

Tables 2–4 list the nondimensional frequencies $\omega a^2 \sqrt{\rho h/D}$ of plates ($h/a = 0.1$), produced using different numbers of admissible functions, with C-F-F boundary conditions and having $\alpha = 90°$, $270°$ and $355°$, respectively. Notably, increasing the vertex angle leads to more severe stress singularities at the neighborhood of $r = 0$. It can be observed that the results for the plate with $\alpha = 90°$ converge well even using only algebraic-trigonometric polynomials, but that this is not the case for the plates with $\alpha = 270°$ and $355°$. Adding corner functions to the admissible functions accelerates the convergence of the numerical results considerably, especially for larger α, where the stress singularities are more severe. Using 20 corner functions for each of $\Psi_{r\,c}$, $\Psi_{\theta\,c}$ and W_c and setting $I_2 = I_4 = I_6 = I_8 = 22$ and $I_1 = I_3 = I_5 = I_7 = 21$ in equations (4) gives results that are accurate to at least three significant figures. Table 4 ($\alpha = 355°$) shows that using 800 polynomial terms without any corner functions, the fundamental frequency obtained is 39 percent higher than the accurate value (1.712) obtained when 60 corner functions are added. It is worth noting that using I_k larger than those given in Tables 2–4 may cause numerical difficulties through ill-conditioned matrices.

Table 3. Convergence of $\omega a^2 \sqrt{\rho h/D}$ for a sectorial plate with C-F-F boundary conditions and $\alpha = 270°$.

Mode no.	No. of corner functions	(I_{even}, I_{odd}) in Eqs.(5)				
		(16,15)	(18,17)	(20,19)	(22,21)	(24,23)
	$(\Psi_{r\,c}, \Psi_{\theta\,c}, W_c)$	437[#]	546[#]	667[#]	800[#]	945[#]
1	(0,0,0)	2.482	2.425	2.388	2.359	2.335
	(10,10,10)	2.191	2.036	1.983	1.966	1.965
	(20,20,20)	2.032	2.012	1.966	1.964	1.962
2	(0,0,0)	2.974	2.906	2.832	2.804	2.774
	(10,10,10)	2.484	2.296	2.225	2.204	2.201
	(20,20,20)	2.299	2.244	2.204	2.200	2.198
3	(0,0,0)	4.684	4.635	4.629	4.617	4.596
	(10,10,10)	4.535	4.468	4.373	4.370	4.368
	(20,20,20)	4.465	4.397	4.369	4.366	4.366
4	(0,0,0)	8.157	8.063	8.046	8.030	8.009
	(10,10,10)	7.868	7.808	7.803	7.795	7.791
	(20,20,20)	7.808	7.804	7.794	7.789	7.787
5	(0,0,0)	12.54	12.50	12.48	12.47	12.45
	(10,10,10)	12.27	12.18	12.16	12.16	12.15
	(20,20,20)	12.19	12.16	12.16	12.15	12.15

Note: "#" denotes the total number of terms in Ψ_{rp}, $\Psi_{\theta p}$ and W_p.

Table 4. Convergence of $\omega a^2 \sqrt{\rho h/D}$ for a sectorial plate with C-F-F boundary conditions and $\alpha = 355°$.

Mode no.	No. of corner functions	(I_{even}, I_{odd}) in Eqs.(5)			
		(16,15)	(18,17)	(20,19)	(22,21)
	$(\Psi_{r\,c}, \Psi_{\theta\,c}, W_c)$	437[#]	546[#]	667[#]	800[#]
1	(0,0,0)	2.504	2.448	2.375	2.319
	(10,10,10)	1.808	1.745	1.717	1.714
	(20,20,20)	1.745	1.714	1.712	1.712
2	(0,0,0)	3.029	2.918	2.839	2.765
	(10,10,10)	2.401	2.286	2.184	2.182
	(20,20,20)	2.304	2.183	2.180	2.177
3	(0,0,0)	3.717	3.654	3.624	3.597
	(10,10,10)	3.421	3.338	3.275	3.272
	(20,20,20)	3.344	3.296	3.267	3.266
4	(0,0,0)	5.452	5.335	5.281	5.237
	(10,10,10)	5.096	4.782	4.735	4.725
	(20,20,20)	5.007	4.733	4.725	4.722
5	(0,0,0)	8.041	7.979	7.927	7.880
	(10,10,10)	7.595	7.383	7.343	7.339
	(20,20,20)	7.385	7.340	7.337	7.336

Note: "#" denotes the total number of terms in Ψ_{rp}, $\Psi_{\theta p}$ and W_p.

Tables 2 to 4 show corner functions accelerating the convergence of the numerical solution, but the corner functions themselves are rather too complicated. Can one use some simplified corner functions having the same singular order as the original corner functions and get accurate results? To answer this question, a simple convergence study was conducted for F-F-F and C-F-F sectorial plates with $\alpha = 355°$ and $h/a = 0.1$. Tables 5 and 6 show the results obtained by using the corner functions given in Table 1 and by using simplified corner functions defined as follows:

For clamped-free radial edges,

$$\Psi_{rc}(r, \theta) \quad = \quad g_1(r) \sum_{k=1}^{K} r^{\mathrm{Re}[\lambda_k]} \{\overline{B}_k \sin(\mathrm{Re}[\lambda_k]\theta) + \hat{B}_k \theta \cos(\mathrm{Re}[\lambda_k]\theta)\}, \tag{9a}$$

$$\Psi_{\theta c}(r, \theta) \quad = \quad g_2(r) \sum_{k=1}^{K} r^{\mathrm{Re}[\lambda_k]} \{\bar{C}_k \sin(\mathrm{Re}[\lambda_k]\theta) + \hat{C}_k \theta \cos(\mathrm{Re}[\lambda_k]\theta)\}, \tag{9b}$$

$$W_c(r, \theta) \quad = \quad g_3(r) \sum_{k=1}^{K} \overline{A}_k r^{\bar{\lambda}_k} \sin(\bar{\lambda}_k \theta). \tag{9c}$$

For free-free radial edges,

$$\Psi_{rc,S}(r, \theta) \quad = \quad g_1(r) \sum_{k=1}^{K} \hat{B}_k r^{\mathrm{Re}[\lambda_k]} \cos(\mathrm{Re}[\lambda_k]\theta), \tag{10a}$$

$$\Psi_{\theta c,S}(r, \theta) \quad = \quad g_2(r) \sum_{k=1}^{K} \bar{C}_k r^{\mathrm{Re}[\lambda_k]} \sin(\mathrm{Re}[\lambda_k]\theta), \tag{10b}$$

$$W_{c,S}(r, \theta) \quad = \quad g_3(r) \sum_{k=1}^{K} \hat{A}_k r^{\bar{\lambda}_k} \cos(\bar{\lambda}_k \theta), \tag{10c}$$

and

$$\Psi_{rc,A}(r, \theta) \quad = \quad g_1(r) \sum_{k=1}^{K} \overline{B}_k r^{\mathrm{Re}[\lambda_k]} \sin(\mathrm{Re}[\lambda_k]\theta), \tag{11a}$$

$$\Psi_{\theta c,A}(r, \theta) \quad = \quad g_2(r) \sum_{k=1}^{K} \hat{C}_k r^{\mathrm{Re}[\lambda_k]} \cos(\mathrm{Re}[\lambda_k]\theta)\}, \tag{11b}$$

$$W_{c,A}(r, \theta) \quad = \quad g_3(r) \sum_{k=1}^{K} \overline{A}_k r^{\bar{\lambda}_k} \sin(\bar{\lambda}_k \theta), \tag{11c}$$

where the subscripts ",S" and ",A" denote the symmetric and antisymmetric modes, respectively. These simplified corner functions give the correct singularity orders of moments and shear forces at $r = 0$. The simplified corner functions for $\Psi_{r\,c}$ and $\Psi_{\theta\,c}$ are much simpler than the original corner functions, especially those for clamped-free radial edges.

Table 5. Comparison of $\omega a^2 \sqrt{\rho h/D}$ for a completely free sectorial plate with $\alpha = 355°$ and $h/a = 0.1$ by using different corner functions.

Mode no.	No. of corner functions $(\Psi_{r\,c}, \Psi_{\theta\,c}, W_c)$	$(I_{\text{even}}, I_{\text{odd}})$ in Eqs.(5)				
		(16, 15)	(18,17)	(20,19)	(22,21)	(24,23)
1	(0,0,0)	5.261	5.244	5.242	5.240	5.237
(A)	(1,1,1)	4.875	4.814	4.779	4.755	4.750
		[4.890]	[4.819]	[4.783]	[4.758]	[4.752]
	(5,5,5)	2.782	2.760	2.747	2.740	2.736
		[2.795]	[2.763]	[2.752]	[2.746]	[2.740]
2	(0,0,0)	5.345	5.301	5.297	5.296	5.294
(S)	(1,1,1)	4.713	4.690	4.642	4.601	4.579
		[4.721]	[4.695]	[4.649]	[4.607]	[4.596]
	(5,5,5)	4.268	4.241	4.234	4.232	4.231
		[4.277]	[4.246]	[4.239]	[4.237]	[4.235]
3	(0,0,0)	8.881	8.854	8.849	8.843	8.839
(S)	(1,1,1)	8.010	7.980	7.936	7.894	7.845
		[8.024]	[7.988]	[7.940]	[7.899]	[7.850]
	(5,5,5)	7.645	7.561	7.556	7.551	7.547
		[7.659]	[7.566]	[7.560]	[7.556]	[7.551]
4	(0,0,0)	12.02	12.00	11.99	11.98	11.98
(A)	(1,1,1)	10.25	10.18	10.09	10.02	10.00
		[10.27]	[10.19]	[10.10]	[10.03]	[10.02]
	(5,5,5)	7.653	7.609	7.596	7.592	7.589
		[7.667]	[7.616]	[7.603]	[7.599]	[7.594]
5	(0,0,0)	12.12	12.12	12.12	12.11	12.11
(S)	(1,1,1)	11.51	11.51	11.50	11.49	11.49
		[11.52]	[11.52]	[11.51]	[11.51]	[11.51]
	(5,5,5)	11.26	11.24	11.23	11.23	11.22
		[11.27]	[11.25]	[11.24]	[11.23]	[11.23]

Note: (S) and (A) denote symmetric and antisymmetric modes, respectively. [] represents the results obtained by using simplified corner functions.

In Tables 5 and 6, using one corner function in each $\Psi_{r\,c}$, $\Psi_{\theta\,c}$ and W_c means that only the functions leading to the correct singularity orders of moments and shear forces are added into the admissible functions. When λ_k ($k = 1$) is complex, the real part of the corresponding complex corner function is used if only one corner function is used in the admissible functions. In the case of completely free sectorial plates (Table 5), the simplified corner functions give results very close (within 0.5%) to those produced by the original corner functions (Table 1), although the latter give slightly better solutions. In the case of sectorial plates with C-F-F boundary conditions (see Table 6), the simplified corner functions improve the convergence of the numerical results when compared with the model using just the polynomials. However, the improvement achieved by using the original corner functions is much better; the difference can be more than 4%. The reason for the simplified corner functions having

Table 6. Comparison of $\omega a^2 \sqrt{\rho h/D}$ for a C-F-F sectorial plate with $\alpha = 355°$ and $h/a = 0.1$ by using different corner functions.

Mode no.	No. of corner functions $(\Psi_{r\,c}, \Psi_{\theta\,c}, W_c)$	(I_{even}, I_{odd}) in Eqs.(5)				
		(16,15)	(18,17)	(20,19)	(22,21)	(24,23)
1	(0,0,0)	2.504	2.448	2.375	2.319	2.263
	(1,1,1)	2.388	2.237	2.187	1.932	1.895
		[2.428]	[2.302]	[2.200]	[1.993]	[1.955]
	(5,5,5)	2.216	2.186	1.884	1.851	1.811
		[2.264]	[2.201]	[1.958]	[1.929]	[1.885]
2	(0,0,0)	3.029	2.918	2.839	2.765	2.744
	(1,1,1)	2.857	2.571	2.473	2.416	2.380
		[2.914]	[2.689]	[2.598]	[2.518]	[2.490]
	(5,5,5)	2.513	2.422	2.409	2.377	2.294
		[2.607]	[2.455]	[2.429]	[2.416]	[2.372]
3	(0,0,0)	3.717	3.654	3.624	3.597	3.474
	(1,1,1)	3.625	3.526	3.485	3.463	3.352
		[3.641]	[3.604]	[3.564]	[3.518]	[3.431]
	(5,5,5)	3.510	3.489	3.464	3.345	3.319
		[3.595]	[3.537]	[3.521]	[3.412]	[3.370]
4	(0,0,0)	5.452	5.335	5.281	5.237	5.196
	(1,1,1)	5.298	5.223	5.149	5.112	5.048
		[5.305]	[5.278]	[5.191]	[5.166]	[5.139]
	(5,5,5)	5.185	5.139	5.116	4.988	4.961
		[5.252]	[5.207]	[5.139]	[5.078]	[5.005]
5	(0,0,0)	8.041	7.979	7.927	7.880	7.822
	(1,1,1)	7.918	7.839	7.810	7.761	7.717
		[7.950]	[7.926]	[7.875]	[7.839]	[7.794]
	(5,5,5)	7.762	7.633	7.536	7.498	7.463
		[7.816]	[7.701]	[7.623]	[7.568]	[7.541]

Note: [] represents the results obtained by using simplified corner functions.

different effects on improving the accuracy of the results given in Tables 5 and 6 is that the first few values of λ_k for clamped-free radial edges are complex numbers, so that the simplified corner functions do not correctly portray the singular behaviors of moments in the vicinity of the vertex. Complex λ_k ($k = 1$) yields bending moments approaching infinity in an oscillatory manner as r approaches zero, while the simplified corner functions yield the moments approaching infinity monotonically. The results in Tables 5 and 6 imply that the ability of the corner functions to accurately describe the singular behaviors of moments and shear forces can considerably accelerate the convergence of numerical results. This observation also suggests a need for caution in the use of r^λ-type singular elements in a finite element approach, in which λ is assigned to be real. Notably, the corner functions can cooperate with a finite element approaches as Gifford and Hilton (1978) developed enriched finite elements for determining stress intensity factor in plane crack problems.

Table 7. Frequency parameters $\omega a^2 \sqrt{\rho h/D}$ for completely clamped sectorial plates.

h/a	α (degrees)	Mode Number				
		1	2	3	4	5
0.1	90	42.78	72.01	83.94	105.2	122.4
		[42.75]	[71.96]	[83.86]	[105.1]	[122.2]
	180	25.94	37.46	51.20	61.10	66.32
		[25.91]	[37.43]	[51.16]	[61.06]	[66.26]
	270	21.64	27.63	35.71	44.70	53.90
		[21.62]	[27.60]	[35.68]	[44.66]	[53.87]
	330	20.37	24.43	30.53	37.45	44.88
		[20.35]	[24.40]	[30.51]	[37.43]	[44.85]
0.2	90	33.31	52.06	59.20	72.17	81.72
		[33.28]	[52.04]	[59.16]	[72.14]	[81.71]
	180	21.66	30.08	39.63	45.57	49.60
		[21.63]	[30.06]	[39.61]	[45.53]	[49.55]
	270	18.18	23.09	29.10	35.46	40.91
		[18.14]	[23.07]	[29.07]	[35.43]	[40.88]
	330	16.97	20.75	25.38	30.46	35.69
		[16.95]	[20.71]	[25.36]	[30.42]	[35.66]

Note: [ ] represents results of Liu and Liew (1999).

4. FREQUENCIES AND MODE SHAPES

Extensive convergence studies were performed to give the accurate nondimensional frequency parameters $\omega a^2 \sqrt{\rho h/D}$ listed in Tables 7–9. All frequency results are guaranteed upper bounds to the exact values and exact (i.e., converged) to at least three significant figures. Tables 7–9 list the nondimensional frequencies of the first five modes for sectorial plates with different boundary conditions (C-C-C, F-F-F, C-F-F, S-F-F, C-C-F, and S-C-F), vertex angles ($\alpha = 90°$, $180°$, $270°$ $300°$, $330°$ and $355°$) and ratios of thickness to radius ($h/a = 0.1$ and 0.2). Since there are no published results for thick sectorial plates with $\alpha \geq 180°$ and boundary conditions other than simply supported along the radial edges, the results given in Tables 7–9 emphasize cases where $\alpha \geq 180°$ to fill the gap in existing frequency data in the published literature. Tables 8 and 9, together with the results given in Huang et al. (1994) represent all the possible cases when the circular edge is free.

As mentioned in the introduction, some researchers have investigated the vibrations of annular sector plates and used the free boundary conditions along the inner circular edge and a very small inner to outer radius ratio (0.00001) to approximate the solutions of sectorial plates. The accuracy of these approximate solutions depends on the chosen inner to outer radius ratio and the boundary conditions used along the inner circular edge. It is interesting to compare those published results with the present results, as Leissa et al. (1993) did with their results. Table 7 compares the present results with those of Liu and Liew (1999) for completely clamped sectorial plates. The agreement between the results is excellent, although the results produced by Liu and Liew are always smaller than the present results, as

Table 8. Frequency parameters $\omega a^2 \sqrt{\rho h / D}$ for sectorial plates with $h/a = 0.1$ and having various boundary conditions.

Boundary conditions	α (degrees)	Mode Number				
		1	2	3	4	5
F-F-F	90	15.37	22.00	28.66	35.25	51.66
	180	6.813	9.146	17.30	17.37	27.35
	270	4.454	5.859	9.063	12.29	16.40
	300	3.675	5.378	8.155	10.29	15.01
	330	3.101	4.757	7.737	8.679	12.73
	355	2.730	4.228	7.548	7.577	11.23
C-F-F	90	4.400	12.71	23.06	32.20	47.77
	180	2.388	3.817	8.971	15.53	18.50
	270	1.962	2.198	4.366	7.787	12.15
	300	1.937	2.198	3.839	6.411	10.05
	330	1.802	2.180	3.317	5.373	8.432
	355	1.712	2.177	3.266	4.722	7.336
S-F-F	90	9.055	17.13	27.09	42.39	48.79
	180	2.726	7.342	14.02	16.59	22.63
	270	2.161	3.350	6.681	11.01	15.99
	300	2.156	2.744	5.423	9.059	13.34
	330	1.891	2.868	4.268	7.589	11.33
	355	1.613	2.987	3.742	6.605	10.93
C-C-F	90	13.36	29.81	41.53	56.75	72.98
	180	4.462	8.789	16.81	24.64	24.93
	270	3.066	4.074	7.851	11.12	17.63
	300	2.920	3.461	6.109	10.08	14.13
	330	2.839	3.062	5.113	8.306	11.76
	355	2.688	2.858	3.947	7.240	10.83
S-C-F	90	8.881	25.45	37.66	48.54	69.31
	180	2.899	7.155	14.14	22.99	23.40
	270	2.403	3.281	6.591	10.90	16.17
	300	2.238	3.156	5.415	8.909	13.30
	330	2.027	3.055	4.116	7.497	11.23
	355	1.815	2.847	3.794	7.232	10.81

they used a free boundary condition along the inner circular edge, which makes the plate less constrained than a completely clamped sectorial plate.

Notably, Tables 8 and 9 do not list the zero frequencies of the three rigid body modes and one rigid body mode for plates with F-F-F and S-F-F boundary conditions, respectively. If these rigid body modes are taken into account, as the boundary conditions change from F-F-F to S-F-F, C-F-F, S-C-F, and to C-C-F, the plates become stiffer, so that their frequencies increase for each mode. As the vertex angle (α) increases, the nondimensional frequency parameters generally decrease (except for the second modes of S-F-F plates). This trend was also observed in the solutions based on thin plate theory (McGee et al., 2003).

Table 9. Frequency parameters $\omega a^2 \sqrt{\rho h/D}$ for sectorial plates with $h/a = 0.2$ and having various boundary conditions.

Boundary conditions	α (degrees)	Mode Number				
		1	2	3	4	5
F-F-F	90	14.82	21.31	27.45	33.10	47.30
	180	6.724	8.997	16.39	16.51	25.81
	270	4.376	5.765	8.927	11.99	15.65
	300	3.590	5.286	8.021	10.05	14.47
	330	3.057	4.637	7.645	8.481	11.98
	355	2.632	4.152	7.430	7.458	10.98
C-F-F	90	4.326	12.38	22.14	30.06	44.59
	180	2.296	3.713	8.801	15.19	18.10
	270	1.905	2.134	4.258	7.556	11.85
	300	1.868	2.130	3.822	6.202	9.700
	330	1.758	2.127	3.230	5.261	8.246
	355	1.659	2.121	3.184	4.497	6.725
S-F-F	90	8.573	15.79	24.11	36.75	40.74
	180	2.624	6.835	13.01	15.58	20.60
	270	1.993	3.147	6.475	10.00	14.97
	300	1.954	2.541	5.218	8.691	12.32
	330	1.710	2.656	4.064	7.312	10.81
	355	1.431	2.774	3.538	6.298	10.42
C-C-F	90	11.35	24.77	32.49	40.70	52.90
	180	4.198	8.479	14.80	20.62	21.90
	270	2.823	3.779	7.144	10.11	15.66
	300	2.717	3.187	5.530	9.469	13.11
	330	2.657	2.750	4.601	7.898	10.74
	355	2.474	2.566	3.454	6.930	10.09
S-C-F	90	8.289	23.32	31.60	40.04	52.72
	180	2.649	6.685	12.99	20.57	20.96
	270	2.271	3.078	6.284	9.887	13.16
	300	2.056	2.953	5.210	8.671	12.28
	330	1.829	2.747	3.821	7.247	10.70
	355	1.613	2.561	3.374	6.929	9.738

The effect of thickness on the vibration frequencies can be seen from the results in Tables 8 and 9 and those for thin plates given by McGee et al. (1995b, 2003). The nondimensional frequency parameters decrease as the thickness increases if the radius (a) remains fixed. This is expected, because the effects of shear deformation and rotary inertia are included here. However, if h increases, with all other parameters (ρ, E, υ) remaining the same, the frequencies (ω) also increase.

Figures 2 to 4 show the nodal patterns of the first five modes for sectorial plates having $h/a = 0.1$ and the same vertex angles ($\alpha = 90°$, $180°$, $270°$ $300°$, $330°$, and $355°$) as in Tables 8 and 9 and various boundary conditions (F-F-F, C-F-F, and C-C-F). The parenthesized numbers are the nondimensional frequencies for the corresponding modes. The nodal
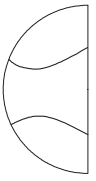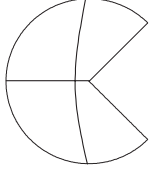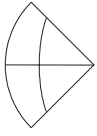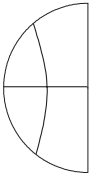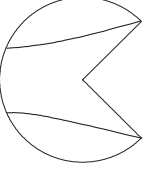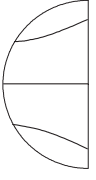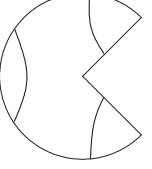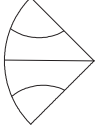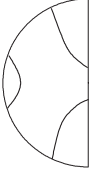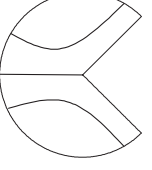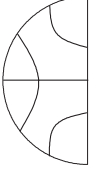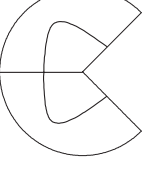
Mode number	α		
	90	180	270
1	(15.37)	(6.813)	(4.454)
2	(22.00)	(9.146)	(5.859)
3	(28.66)	(17.30)	(9.063)
4	(35.25)	(17.37)	(12.29)
5	(51.66)	(27.35)	(16.40)

Figure 2. Nodal patterns for F-F-F sectorial plates with $h/a = 0.1$ and various vertex angles.
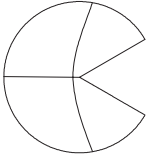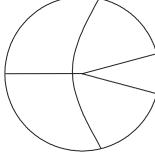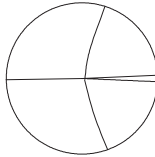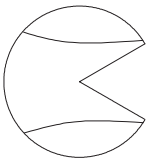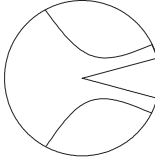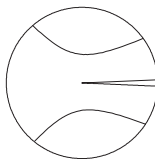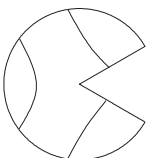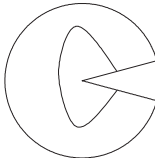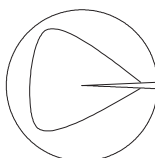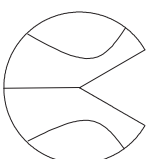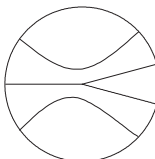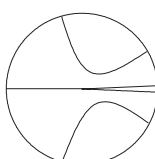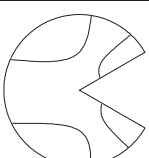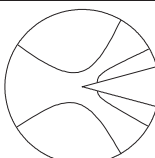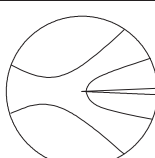
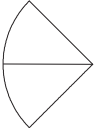| Mode number	α		
	300	330	355
1	(3.675)	(3.101)	(2.730)
2	(5.378)	(4.757)	(4.228)
3	(8.155)	(7.737)	(7.548)
4	(10.29)	(8.679)	(7.577)
5	(15.01)	(12.73)	(11.23)

Figure 2. Nodal patterns for F-F-F sectorial plates with $h/a = 0.1$ and various vertex angles. *(Continued)*

patterns of the F-F-F and C-F-F sectorial plates with $\alpha = 355°$ shown in Figures 2 and 3 are very similar to those for thin plates given by Leissa et al. (1993) and McGee et al. (1995), respectively. The existence of the sharp V-notch ($\alpha = 355°$) severely distorts the nodal patterns of a completely free circular plate. When α changes from 330° to 355°, the nodal patterns for F-F-F plates remain very similar, and the nodal patterns for C-F-F plates are also similar except for the third mode, but the nodal patterns of the first three modes for C-C-F plates change dramatically.
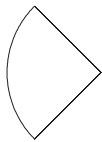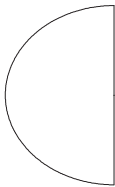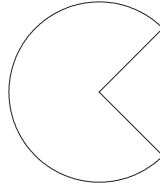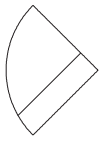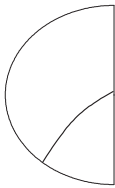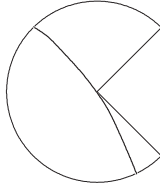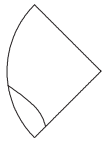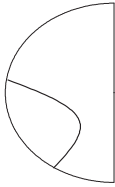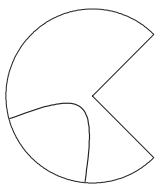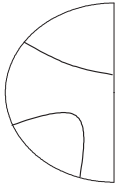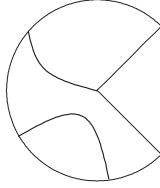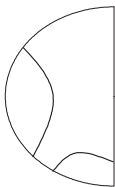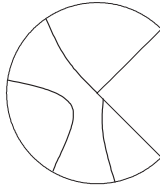
Mode number	α		
	90	180	270
1	(4.400)	(2.388)	(1.962)
2	(12.71)	(3.817)	(2.198)
3	(23.06)	(8.971)	(4.366)
4	(32.20)	(15.53)	(7.787)
5	(47.77)	(18.50)	(12.15)

Figure 3. Nodal patterns for C-F-F sectorial plates with $h/a = 0.1$ and various vertex angles.
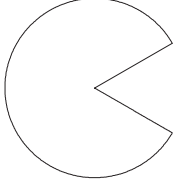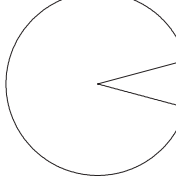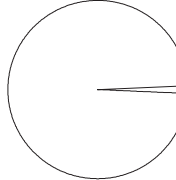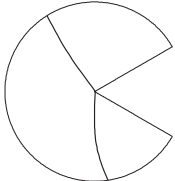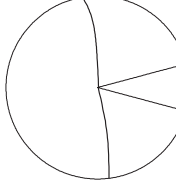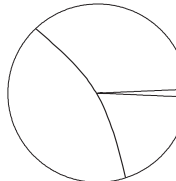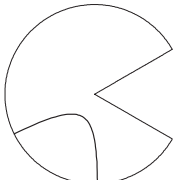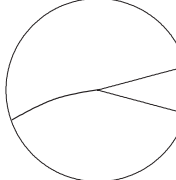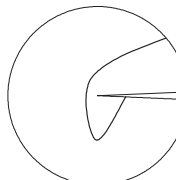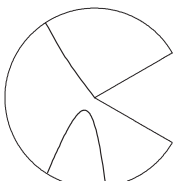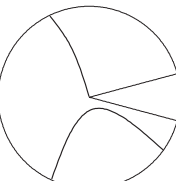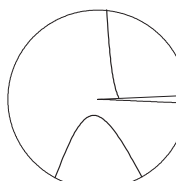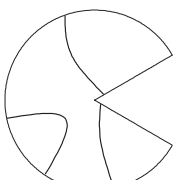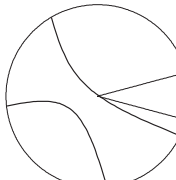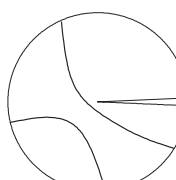
Mode number	α		
	300	330	355
1	(1.937)	(1.802)	(1.712)
2	(2.198)	(2.180)	(2.177)
3	(3.839)	(3.317)	(3.266)
4	(6.411)	(5.373)	(4.722)
5	(10.05)	(8.432)	(7.336)

Figure 3. Nodal patterns for C-F-F sectorial plates with $h/a = 0.1$ and various vertex angles. *(Continued)*
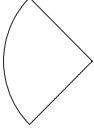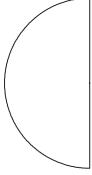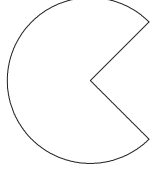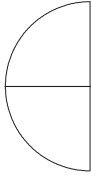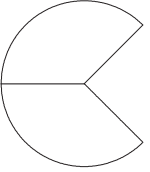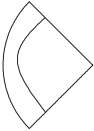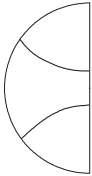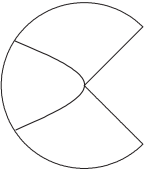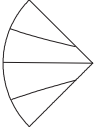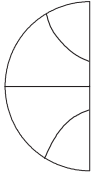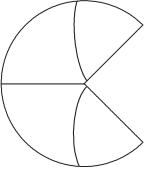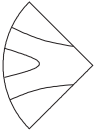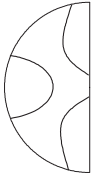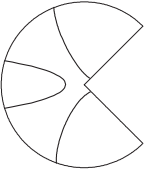
Mode number	α		
	90	180	270
1	(13.36)	(4.462)	(3.066)
2	(29.81)	(8.789)	(4.074)
3	(41.53)	(16.81)	(7.851)
4	(56.75)	(24.64)	(11.12)
5	(72.98)	(24.93)	(17.63)

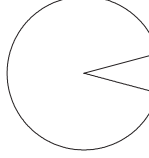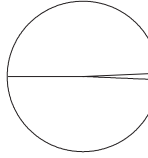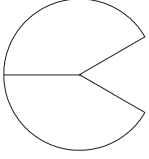Figure 4. Nodal patterns for C-C-F sectorial plates with $h/a = 0.1$ and various vertex angles.
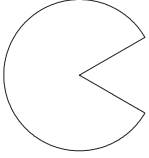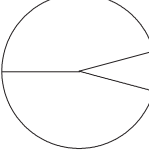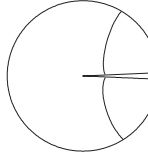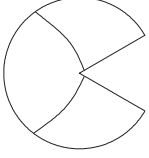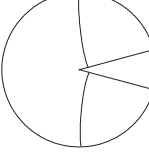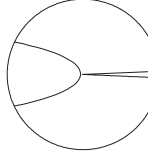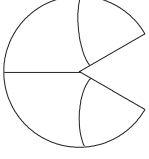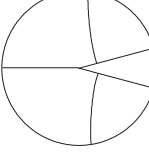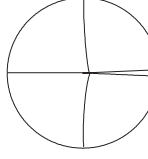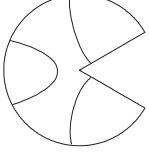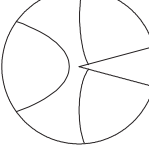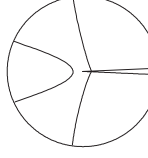
Mode number	α		
	300	330	355
1	(2.920)	(2.839)	(2.688)
2	(3.461)	(3.062)	(2.858)
3	(6.109)	(5.113)	(3.947)
4	(10.08)	(8.306)	(7.240)
5	(14.13)	(11.76)	(10.83)

Figure 4. Nodal patterns for C-C-F sectorial plates with $h/a = 0.1$ and various vertex angles. *(Continued)*

The increase of vertex angle changes the sequence of the mode shapes for the symmetric and antisymmetric modes of F-F-F and C-C-F plates. For example, for F-F-F boundary conditions, the first modes of the plates with $\alpha = 90°$ and $180°$ are symmetric modes while the first modes for $\alpha = 270°$, $300°$, $330°$ and $355°$ are antisymmetric modes. The opposite sequence of symmetric and antisymmetric modes with changing α is observed for the second modes. For C-C-F boundary conditions, the first modes of the plates with $\alpha = 90°$, $180°$,

270°, 300°, and 330° are symmetric modes with no nodal line, while the mode without a nodal line disappears for the case of $\alpha = 355°$, the first mode of which is an antisymmetric mode. These changes do not alter the trend of frequencies decreasing with the increase of the vertex angle.

5. CONCLUSION

This paper has demonstrated that adding corner functions to the algebraic-trigonometric polynomials as admissible functions of the Ritz method can significantly accelerate the convergence of the numerical results for sectorial plates. The main effect of the corner functions is to accurately present the singular behaviors of moments and shear forces in the vicinity of the vertex. When the moments or shear forces approach infinity in an oscillatory manner in the neighborhood of the vertex (i.e., when λ_k is complex), the admissible functions must not only have the correct singularity order for the moments or shear forces, but also show the correct oscillation behavior.

Detailed numerical tables have been presented for frequencies of moderately thick sectorial plates ($h/a = 0.1$ and 0.2) with various boundary conditions and vertex angles. The presented frequencies are all exact to at least three significant figures and are, in most cases, the first such results to be shown in the published literature, as are the nodal patterns also given here. Generally speaking, the vibration frequencies decrease as the vertex angle increases. The nondimensional frequencies $\omega a^2 \sqrt{\rho h / D}$ decrease as the thickness of the plate increases. This reliable information serves not only to improve the understanding of how sectorial plates can vibrate, but also as benchmark data against which other computational methods (such as finite element, boundary element or differential quadrature methods) may be checked.

Although this paper only considers the vibrations of sectorial plates, the method used here can be easily extended to study the vibration behaviors of a circular plate with V-notches (or cracks), where the notch vertex is not at the circle center.

REFERENCES

Bhattacharya, A. P. and Bhowmic, K. N., 1975, "Free vibration of a sectorial plate," *Journal of Sound and Vibration* **41**(4), 503–505.

Cheung, M. S. and Chan, M. Y. T., 1981, "Static and dynamic analysis of thin and thick sectorial plates by the finite strip method," *Computers and Structures* **14**, 79–88.

Gifford, L. N., Jr. and Hilton, P. D., 1978, "Stress intensity factors by enriched finite elements," *Engineering Fracture Mechanics* **10**, 485–496.

Guruswamy, P. and Yang, T. Y., 1979, "A sector finite element for dynamic analysis of thick plates," *Journal of Sound and Vibration* **62**(4), 505–516.

Houmat, A., 2001, "A sector Fourier p-element applied to free vibration analysis of sectorial plates," *Journal of Sound and Vibration* **243**(2), 269–282.

Huang, C. S., Leissa, A. W., and McGee, O. G., 1993, "Exact analytical solutions for the vibrations of sectorial plates with simply supported radial edges," *Journal of Applied Mechanics* **60**(2), 478–483.

Huang, C. S., McGee, O. G., and Leissa, A. W., 1994, "Exact analytical solutions for free vibrations of thick sectorial plates with simply supported radial edges," *International Journal of Solids and Structures* **31**, 1609–1631.

Huang, C. S., 2003, "Stress singularities at angular corners in first-order shear deformation plate theory," *International Journal of Mechanical Sciences* **45**(1), 1–20.

Huang, C. S., Leissa, A. W., Chang, M. J., 2005, "Vibrations of skewed cantilevered triangular, trapezoidal and parallelogram Mindlin plates with considering corner stress singularities," *International Journal for Numerical Methods in Engineering* **62**(13),1789–1806.

Leissa, A. W., 1969, Vibration of Plates. NASA SP-160, U.S. Government Printing Office. Reprinted, Acoustical Society of America, 1993.

Leissa, A. W., 1977a, "Recent research in plate vibrations, 1973–1976: Classical theory," *The Shock and Vibration Digest* **9**(10), 13–24.

Leissa, A. W., 1977b," Recent research in plate vibrations: Complicating effects," *The Shock and Vibration Digest* **9**(11), 21–35.

Leissa, A. W., 1981a, "Plate vibration research, 1976–1980: Classical theory," *The Shock and Vibration Digest* **13**(9), 11–22.

Leissa, A. W., 1981b, "Plate vibration research, 1976–1980: Complicating effects," *The Shock and Vibration Digest* **13**(10), 19–36.

Leissa, A. W., 1987a, "Recent studies in plate vibrations: 1981–1985. Part I. Classical theory," *The Shock and Vibration Digest* **19**(2), 11–18.

Leissa, A. W., 1987b, "Recent research in plate vibrations, 1981–1985, Part II: Complicating effects," *The Shock and Vibration Digest* **19**(3), 10–24.

Leissa, A. W., McGee, O. G., and Huang, C. S., 1993, "Vibrations of sectorial plates having corner stress singularities," *Journal of Applied Mechanics* **60**, 478–483.

Liew, K. M. and Liu, F.-L., 2000, "Differential quadrature method for vibration analysis of shear deformable annular sector plates," *Journal of Sound and Vibration* **230**(2), 335–356.

Liew, K. M., Xiang, Y., and Kitipornchai, S., 1995, "Research on thick plate vibration: a literature survey," *Journal of Sound and Vibration* **180**(1), 163–176.

Liu, F.-L. and Liew, K. M., 1999, "Free vibration analysis of Mindlin sector plates: numerical solutions by differential quadrature method," *Computer Methods in Applied Mechanics and Engineering* **177**, 77–92.

Maruyama, K. and Ichinomiya, O., 1981, "Experimental Investigation of free vibrations of clamped sector plates," *Journal of Sound and Vibration* **74**(4), 565–573.

McGee, O. G., Huang, C. S., and Leissa, A. W., 1995a, "Comprehensive exact solutions for free vibrations of thick annular sectorial plates with simply supported radial edges," *International Journal of Mechanical Sciences* **37**(5), 537–566.

McGee, O. G., Leissa, A. W., Huang, C. S., and Kim, J. W., 1995b, "Vibrations of circular plates with clamped V-notches or rigidly constrained radial cracks," *Journal of Sound and Vibration* **181**(2), 185–201.

McGee, O. G., Leissa, A. W., Kim, J. W., and Kim, Y. S., 2003, "Vibration of plates with constrained V-notches or cracks," *Journal of Engineering Mechanics* **129**(7), 812–822.

McGee, O. G., Kim, J. W., and Leissa, A. W., 2005, "Sharp corner functions for Mindlin plates," *Journal of Applied Mechanics* **72**(1), 1–9.

Mizusawa, T., 1991, "Vibration of thick annular sector plates using semi-analytical methods," *Journal of Sound and Vibration* **150**(2), 245–259.

Mizusawa, T., Kito, H., and Kajita, T., 1994, "Vibration of annular sector Mindlin plates by the spline strip method," *Computers & Structures* **53**(5), 1205–1215.

Rubin, C., 1975, "Nodal circles and natural frequencies for the isotropic wedge," *Journal of Sound and Vibration* **39**(4), 523–526.

Srinivasan, R. S. and Thiruvenkatachari, V., 1985, "Free vibration of transverse isotropic annular sector Mindlin plates," *Journal of Sound and Vibration* **101**(2), 193–201.

Waller, M. D., 1952, "Vibrations of free plates, line symmetry, corresponding modes," *Proceedings of the Royal Society of London* **A211**, 265–276.

Wang, X. and Wang, Y., 2004, "Free vibration analyses of thin sector plates by the new version of differential quadrature method," *Computational Methods in Applied Mechanics and Engineering* **193**, 3957–3971.

Xiang, Y., Liew, K. M., and Kitipornchai, S., 1993, "Transverse vibration of thick annular sector plates," *Journal of Engineering Mechanics* **119**(8), 1579–1599